

## PDF hosted at the Radboud Repository of the Radboud University Nijmegen

The following full text is a publisher's version.

For additional information about this publication click this link.

<http://hdl.handle.net/2066/175108>

Please be advised that this information was generated on 2021-09-26 and may be subject to change.



## Lung cancer radiotherapy

## Survival prediction of non-small cell lung cancer patients using radiomics analyses of cone-beam CT images



Janna E. van Timmeren<sup>a,\*</sup>, Ralph T.H. Leijenaar<sup>a</sup>, Wouter van Elmpt<sup>a</sup>, Bart Reymen<sup>a</sup>, Cary Oberije<sup>a</sup>, René Monshouwer<sup>b</sup>, Johan Bussink<sup>b</sup>, Carsten Brink<sup>c,d</sup>, Olfred Hansen<sup>c,d,e</sup>, Philippe Lambin<sup>a</sup>

<sup>a</sup> Department of Radiation Oncology (MAASTRO), GROW – School for Oncology and Developmental Biology, Maastricht University Medical Centre (MUMC); <sup>b</sup> Department of Radiation Oncology, Radboud University Medical Center, Nijmegen, The Netherlands; <sup>c</sup> Institute of Clinical Research, University of Southern Denmark, Odense; <sup>d</sup> Laboratory of Radiation Physics, Odense University Hospital; and <sup>e</sup> Department of Oncology, Odense University Hospital, Denmark

## ARTICLE INFO

## Article history:

Received 2 January 2017  
Received in revised form 20 March 2017  
Accepted 17 April 2017  
Available online 12 May 2017

## Keywords:

Radiomics  
Computed tomography  
Cone-beam CT  
Non-small cell lung cancer  
Survival prediction

## ABSTRACT

**Background and purpose:** In this study we investigated the interchangeability of planning CT and cone-beam CT (CBCT) extracted radiomic features. Furthermore, a previously described CT based prognostic radiomic signature for non-small cell lung cancer (NSCLC) patients using CBCT based features was validated.

**Material and methods:** One training dataset of 132 and two validation datasets of 62 and 94 stage I–IV NSCLC patients were included. Interchangeability was assessed by performing a linear regression on CT and CBCT extracted features. A two-step correction was applied prior to model validation of a previously published radiomic signature.

**Results:** 13.3% (149 out of 1119) of the radiomic features, including all features of the previously published radiomic signature, showed an  $R^2$  above 0.85 between intermodal imaging techniques. For the radiomic signature, Kaplan–Meier curves were significantly different between groups with high and low prognostic value for both modalities. Harrell's concordance index was 0.69 for CT and 0.66 for CBCT models for dataset 1.

**Conclusions:** The results show that a subset of radiomic features extracted from CT and CBCT images are interchangeable using simple linear regression. Moreover, a previously developed radiomics signature has prognostic value for overall survival in three CBCT cohorts, showing the potential of CBCT radiomics to be used as prognostic imaging biomarker.

© 2017 The Authors. Published by Elsevier Ireland Ltd. Radiotherapy and Oncology 123 (2017) 363–369  
This is an open access article under the CC BY-NC-ND license (<http://creativecommons.org/licenses/by-nc-nd/4.0/>).

With 1.6 million deaths in 2012, lung cancer is the most common cause of death from cancer worldwide [1,2]. Lung cancer is also the most frequently diagnosed cancer with 1.82 million new cases in 2012, comprising 12.9% of the worldwide incidence. Improved disease outcome and a subsequent increase in a patient's chance of survival can be achieved by individualized treatment [3–5]. To this end, biomarkers are needed [6,7].

Medical imaging has become a cornerstone of personalized cancer treatment over the past decades. Novel advanced imaging analysis techniques such as radiomics – extracting quantitative features from medical images such as computed tomography (CT), positron emission tomography (PET), or magnetic resonance

imaging (MRI) – can identify a patient's response to treatment or the probability of developing side effects [3,8–14].

Furthermore, a longitudinal approach where the change of quantitative radiomic features (i.e. delta radiomics) is examined, may also aid in early response assessment compared to the use of only baseline (imaging) characteristics [15–17]. However, in most studies, PET-, CT- or MRI-scans are only performed at baseline or at very limited number of points in time, hampering the possibility for timely treatment adaptation. However, during radiotherapy for NSCLC patients, three-dimensional (3D) cone-beam CT (CBCT) images are routinely obtained for patient set-up and positioning verification [18]. These images could provide valuable information about day-to-day changes of the tumor during the course of treatment [19].

Radiomics based on CBCT imaging therefore offers a possibility for (early) treatment adaptation using the changes of imaging biomarkers over time. Where the prognostic value of conventional

\* Corresponding author at: Department of Radiation Oncology (MAASTRO Clinic), GROW – School for Oncology and Developmental Biology, Maastricht University Medical Centre, Dr. Tanslaan 12, 6229 ET Maastricht, The Netherlands.

E-mail address: [janita.vantimmeren@maastro.nl](mailto:janita.vantimmeren@maastro.nl) (J.E. van Timmeren).

CT images is already known [9,11,20], the potential of CBCT radiomics still needs to be investigated especially because image quality of CBCT is generally worse compared to conventional CT images. Therefore, in this study we aimed to compare radiomics for CT and CBCT by investigating the interchangeability of radiomic features extracted from both modalities. Furthermore, we validated a previously published CT-based radiomics signature (a Cox regression model based on imaging only, without clinical parameters) [20,21], using three independent CBCT datasets to validate the model and to evaluate the prognostic potential of CBCT imaging compared to CT imaging.

## Methods and materials

### Patients

Three NSCLC cohorts from three different institutes were included in this study. All patients received radiation therapy with curative intent. Patients that received less than 40 Gy were excluded from the analysis. Moreover, patients referred to postoperative radiotherapy or simultaneous treatment of brain metastases were excluded, as well as patients with prior history of lung cancer.

The first dataset consists of 132 stage I-IV patients treated between January 2012 and January 2014 at Maastricht University Medical Center, Maastricht, the Netherlands. Data are provided online on [www.cancer-data.org](http://www.cancer-data.org) [22]. The second dataset consists of 62 stage I-IIIb patients receiving treatment between January 2009 and January 2011 at Radboud University Medical Center, Nijmegen, the Netherlands. The third dataset consists of 94 stage I-IIIb patients, a subset of the cohort used in a previous study on CBCT imaging [19], treated between November 2007 and December 2011 at Odense University Hospital, Odense, Denmark. This retrospective study was approved by each respective institutional review board.

### Image acquisition

The images of the treatment planning CT (pCT) scan and the images of the cone-beam CT (CBCT) scan prior to the first radiotherapy fraction were used for all analyses in this study. Details of all image acquisitions can be found in the Supplementary Material.

### Feature extraction

The gross tumor volume (GTV) of the primary tumor was manually delineated on the CT scan by experienced radiation oncologists and used for treatment planning. For each patient, the GTV was registered to the CBCT image using a deformable transformation field obtained by performing non-rigid registration of the pCT image and the CBCT image [23,24]. Afterward, all contours were visually checked and manually adjusted when necessary by an experienced radiation oncologist.

Radiomic features were extracted from the delineated tumor regions of the pCT and CBCT images. A total of 1119 radiomic features were calculated, divided into five groups: tumor intensity ( $n = 19$ ), texture ( $n = 95$ ), wavelet ( $n = 912$ ), Laplacian of Gaussian ( $n = 74$ ), and shape ( $n = 19$ ). Emphasis was placed on the features of the previously published prognostic radiomic signature: I) tumor intensity: 'Energy', II) texture: 'Gray Level Nonuniformity', III) wavelet: 'Gray Level Nonuniformity HLH', and IV) shape: 'Compactness' [20]. All features were automatically extracted using in-house developed software, using Matlab 2014a (MathWorks, Natick, Massachusetts, U.S.A.). A mathematical description of all features can be found at the end of the Supplementary Material.

### Correction

A two-step correction procedure was performed on CBCT prior to model validation, which will be explained in further detail below. The first step comprises an intensity value correction and the second step is a radiomic feature normalization. The workflow of correcting CBCT is shown in Fig. 1.

Step 1, the intensity correction, was performed to equalize the distribution of the intensity levels between CBCT images. To find the correction factor, the mean intensity level in a region of interest (ROI) of approximately  $5 \text{ cm}^2$  in the heart was derived for each patient in the CBCT image. This ROI was chosen because typical Hounsfield units were known and because an area of this size at that location could be drawn for all images. The reference value was set to 50 HU, since according to literature typical Hounsfield units in myocardium and blood are between 40 and 60 HU [25]. A scaling factor was calculated using  $(\text{mean intensity level} + 1000)/(\text{reference value} + 1000)$ . Correction factors, derived for individual patients, were multiplied with intensity levels of CBCT images prior to feature extraction. In this study we decided to apply the intensity correction for all images, instead of defining a certain range around the reference value of 50 HU within which some intensity values could be accepted.

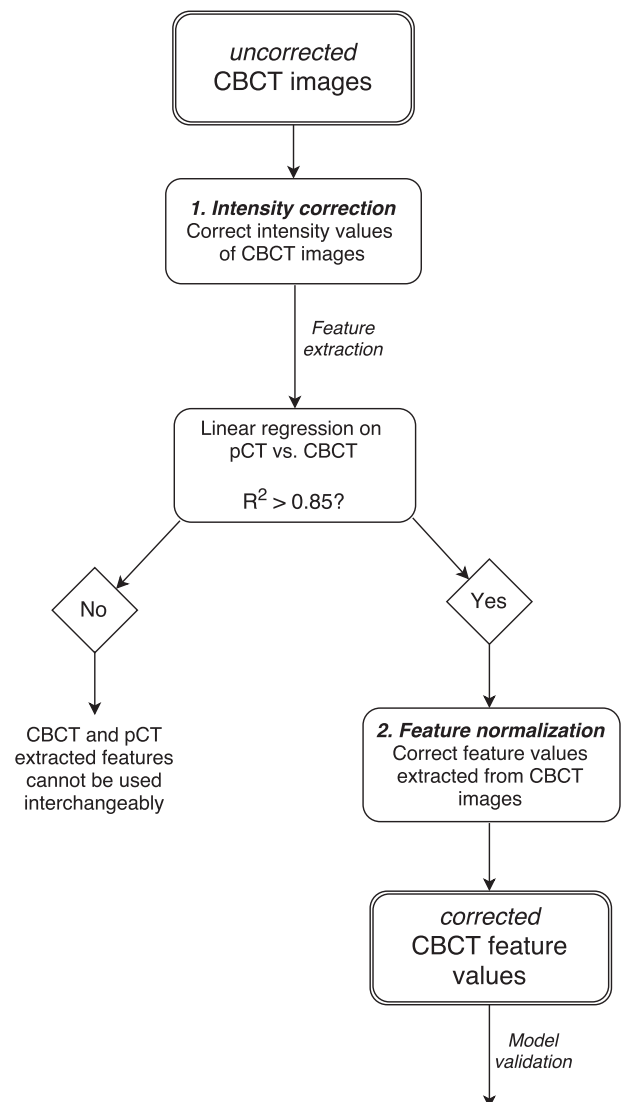


Fig. 1. Workflow. Workflow of two-step correction of CBCT images and extracted features prior to model validation.

Step 2 is the radiomic feature normalization, this was performed to correct CBCT extracted features with a fixed calibration factor in case of a linear relationship between CT and CBCT radiomic feature values. The correction factor was derived by performing a linear regression on the CBCT and pCT extracted features. A coefficient of determination ( $R^2$ ) above 0.85 was considered to indicate a strong linear relationship between pCT and CBCT feature values, meaning that the linear regression parameters (slope and intercept) could be used to correct radiomic feature values derived from CBCT. This procedure was performed for all datasets for the features of the radiomic signature prior to model validation.

The linear regression parameters were used to derive correction factors for feature normalization for the radiomic signature, but at the same time they provide a measure of interchangeability between conventional pCT and CBCT imaging for all radiomic features. Only dataset 1 was used to perform a linear regression on all 1119 radiomic features.

For dataset 1, the slice thickness of all CBCT images matches with the pCT images (3 mm), whereas in datasets 2 and 3 there is discrepancy in slice thicknesses (1 mm for CBCT and 3 mm for pCT). Therefore, analysis of linear regression parameters of the features of the radiomic signature was performed before and after resampling into equal voxel sizes of  $1 \times 1 \times 3$  mm using linear interpolation.

#### Validation of previously published radiomics signature

Model validation was performed on pCT and CBCT images of all datasets to validate its prognostic value and to compare prognostic values of the two modalities. The previously published Cox regression model consisted of 4 radiomic features [20]. Overall survival, measured from the start of radiotherapy, was used as endpoint. Patients alive at the end of follow-up were considered right-censored.

The linear predictors (LP), defined as the sum of each coefficient multiplied by the respective feature value with adjustment for average feature values [20],  $LP = \sum_i \beta_i (x_i - \bar{x}_i)$ , were calculated for pCT and CBCT before and after correction to provide another measure for the interchangeability and to visualize the effect of the two-step correction procedure. The median value of the LP derived from the original dataset was  $-0.11916$  [20], and used to separate patients with high prognostic value (i.e. linear predictor below the median) from patients with low prognostic value.

Model validation was performed on all datasets using multiple methods [26], similar as described in Leijenaar et al. [21]. For the first measure of validation, Cox regression was performed on the prognostic index (PI, defined as  $\sum_i \beta_i x_i$ , equal to LP without adjustment for average feature values) to determine the calibration slope, where a slope equal to 1 means that the relative risk model is still valid and there is no need for recalibration. A log-rank (LR) test was used to test whether the slope was different from 1. Secondly, model fit was evaluated by performing the Cox regression on the individual features of the signature with variable coefficients plus the PI with a fixed coefficient of 1 (i.e. offsetting the PI), and performing a joint test that all feature coefficients are 0. Thirdly, discrimination of the model was assessed by calculating Harrell's concordance index (c-index), ranging from 0.5 (no discrimination) to 1 (perfect discrimination). Finally, Kaplan–Meier curves were made to visualize the potential discrimination between survival curves of groups with high or low prognostic value based on a median prediction threshold of the original model data of Aerts et al. [20] and a LR test was performed to test the significance of the curve split.

To compare the performance of the original model on corrected CBCT to a new model on original CBCT images, the coefficients of the same four variables of the radiomic signature were refitted on the CBCT images of dataset 1 without applying correction step

1 or 2. The performance of this recalibrated model was evaluated for all three datasets.

To investigate the relevance of using this radiomics model for comparing prognostic performance of pCT and CBCT, we compared the model's performance to the recognized prognostic factor 'TNM-stage' for dataset 1. Four dummy variables with T2, T3/4, N1/2 and N3 were created, using T1 and N0 as reference categories. We compared the performance of a model with TNM-stage to the original radiomic signature model and also calculated the performance of a model with both the radiomic signature and TNM-stage. Even though we performed this small comparison with clinical data, we want to emphasize that it was not the purpose of this study to develop a new highly prognostic model incorporating different types of information.

All statistical analyses were performed using R (version 3.2.2 and 3.2.3), using the packages *stats*, *survcomp* and *rms*.

## Results

For 17 CBCT images of dataset 1, the field of view (FOV) did not cover the entire tumor volume, so these patients were excluded from further analyses. Moreover, 13 patients had not enough margin around the tumor volume to be able to calculate any filtered radiomic features without needing to perform padding which required imputing values and were therefore also excluded from the analysis. This resulted in a total of 102 CBCT images available for analysis. In Fig. 2 an example of a treatment planning CT and corresponding kV cone-beam CT image from dataset 1 is shown.

For dataset 2, 6 patients had to be excluded because the registration of the images to transfer the delineated GTV did not work or the tumor was not visible on the CBCT due to blurring or decreased image quality. This resulted in a total of 56 patients available for analysis in dataset 2.

For dataset 3, no patients were excluded.

Clinical variables of all patients included in the analysis are shown in Table 1 in Supplementary Material. All patients, including the stage IV patients who had 1 or 2 metastases, were treated with curative intent.

Prior to model validation, correction was applied on CBCT images and features. The mean intensity level in a ROI in the heart ranged from  $-65$  to  $117$  (median  $17.5$ ) for CBCT images acquired in dataset 1, from  $-364$  to  $225$  (median  $-242$ ) for dataset 2 and from  $-372$  to  $226$  (median  $-113$ ) for dataset 3 (Fig. 1 of Supplementary Material). This shows large variability between patients and explains the why correction step 1, intensity correction, was applied. The distribution of intensity levels in the GTV before and after intensity correction was summarized in histograms for all datasets, shown in Fig. 2 of Supplementary Material.

After intensity value corrections, linear regression was performed on the pCT and CBCT extracted radiomic features.

The coefficient of determination ( $R^2$ ) was calculated for all 1119 radiomic features acquired from dataset 1. A total of 149 out of 1119 (13.3%) features had a  $R^2$  above 0.85. This included 2 out of 19 (10.5%) features from the 'tumor intensity' group, 14 out of 95 (14.7%) features from the 'texture' group, 5 out of 74 (6.8%) from the 'Laplacian of Gaussian' group, 118 out of 912 (12.9%) features from the 'wavelet' group and 10 out of 19 (52.6%) features from the 'shape' group. Scatterplots and linear regression parameters of the 100 features with highest  $R^2$  are shown in Supplementary Material Fig. 3 and Table 1, respectively.

The results of linear regression for the four features of the previously published radiomic signature are shown in Table 3 of the Supplementary Material for all datasets. Scatterplots for CBCT versus pCT for the four radiomic signature features are shown in Fig. 3 for all datasets (using original voxel sizes). The parameters of the

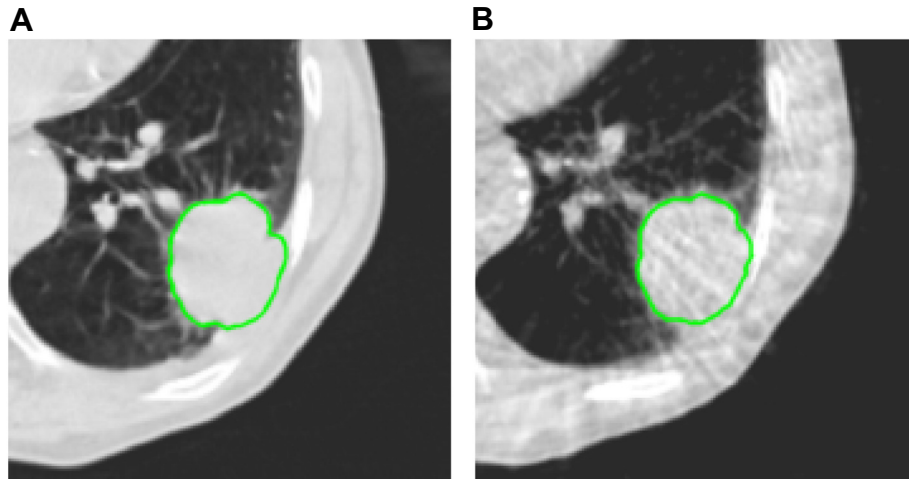


**Fig. 2.** Example of pCT and CBCT image of dataset 1. (A) treatment planning CT scan, (B) kV cone-beam CT scan of the same patient prior to the first fraction of treatment. The GTV is indicated in green. (For interpretation of the references to color in this figure legend, the reader is referred to the web version of this article.)

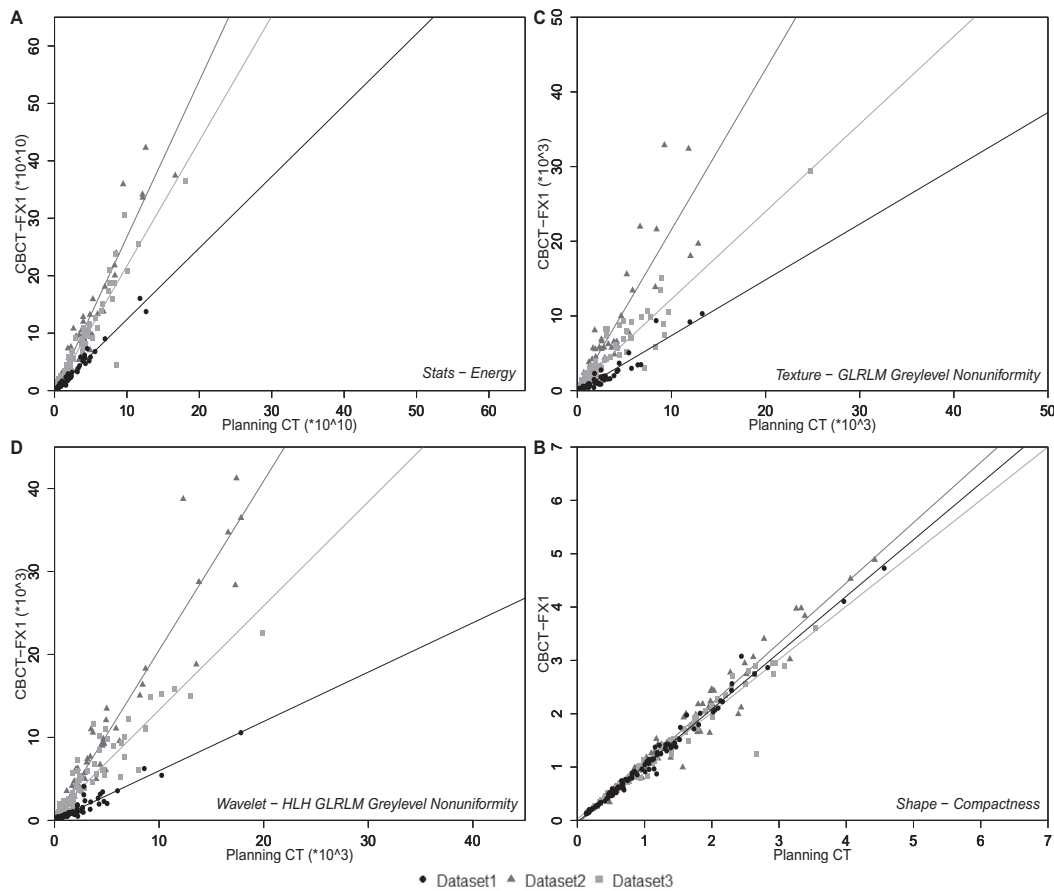


**Fig. 3.** Scatterplots of CBCT extracted radiomic features versus pCT extracted radiomic features. Scatterplots derived for dataset 1 (dots), dataset 2 (triangles) and dataset 3 (squares). (A) Tumor intensity - 'Energy', (B) Texture - 'Gray Level Nonuniformity', (C) Wavelet - 'HLH Gray Level Nonuniformity', (D) Shape - 'Compactness'. GLRLM: Gray Level Run Length Matrix, H: High, L: Low.

linear regression, i.e. the slopes and intercepts, were used to correct CBCT feature values of all CBCT images of that respective dataset (correction step 2).

Linear predictor values of the radiomics signature were derived from CBCT imaging before and after performing the two-step correction method. Linear predictors of individual patients of all datasets are shown in Figs. 4–6 of the Supplementary Material.

After the two-step correction procedure, model validation was performed. All validation statistics are shown in Table 1 for both pCT and CBCT. For dataset 1, the proportion of Stage I patients was relatively large, therefore model validation was performed separately for the patients with Stage I ( $n = 42$ ) and for the patients with Stage II or higher ( $n = 60$ ). These results are shown in Table 4 of Supplementary Material.

**Table 1**

Model validation results for pCT and CBCT for all datasets.

|           |      | Calibration slope on the PI (SE, <i>p</i> -value LR test) | Joint test on all coefficients, <i>p</i> -value | Harrell's c-index (95% CI, <i>p</i> -value)           |
|-----------|------|---|---|---|
| Dataset 1 | pCT  | 1.77 (SE = 0.42, <i>p</i> = 0.09)                         | <i>p</i> = 0.013                                | 0.69 (0.63 – 0.75, <i>p</i> = 9.9*10 <sup>-10</sup> ) |
|           | CBCT | 1.90 (SE = 0.44, <i>p</i> = 0.06)                         | <i>p</i> = 0.027                                | 0.66 (0.59 – 0.73, <i>p</i> = 4.8*10 <sup>-6</sup> )  |
| Dataset 2 | pCT  | 0.90 (SE = 0.28, <i>p</i> = 0.72)                         | <i>p</i> = 0.84                                 | 0.61 (0.52 – 0.70, <i>p</i> = 0.016)                  |
|           | CBCT | 1.17 (SE = 0.33, <i>p</i> = 0.62)                         | <i>p</i> = 0.53                                 | 0.63 (0.54 – 0.72, <i>p</i> = 0.0052)                 |
| Dataset 3 | pCT  | 0.36 (SE = 0.23, <i>p</i> = 0.0017)                       | <i>p</i> = 0.28                                 | 0.59 (0.53 – 0.65, <i>p</i> = 0.0036)                 |
|           | CBCT | 0.73 (SE = 0.30, <i>p</i> = 0.35)                         | <i>p</i> = 0.0024                               | 0.59 (0.53 – 0.66, <i>p</i> = 0.0063)                 |

Significant differences between Kaplan–Meier curves of groups with high and low prognostic value were found for both the pCT cohort and the CBCT cohort (*p* = 0.00064 and *p* = 0.00020, respectively) in dataset 1. For dataset 2, the Kaplan–Meier curves did not split significantly for pCT (*p* = 0.43) and for CBCT (*p* = 0.12). For dataset 3, differences between Kaplan–Meier curves were not significant for both pCT (*p* = 0.05) and CBCT (*p* = 0.19). Survival curves are shown in Fig. 4. Additional Kaplan–Meier curves with different forms and steps of the correction procedure are shown in Figures 7–9 in Supplementary Material for all datasets.

The model consisting of the same four radiomic signature features, but recalibrated on original, uncorrected CBCT images of

dataset 1, achieved a c-index of 0.69 (95% CI 0.63–0.75, *p* = 4.0 \* 10<sup>-10</sup>) for dataset 1, a c-index of 0.43 (95% CI 0.34–0.51, *p* = 0.08) for dataset 2 and 0.45 (95% CI 0.38–0.52, *p* = 0.16) for dataset 3 (all uncorrected images). All other statistics also showed that this recalibrated model could not be validated on original CBCT images of dataset 2 and 3 (not shown).

For dataset 1, the c-index of TNM-stage was found to be 0.62 (95% CI 0.54–0.71, *p* = 0.0044), but model performance of the radiomic signature did not improve when including staging in the original model, with a c-index of 0.66 (95% CI 0.58–0.73, *p* = 2.0\*10<sup>-5</sup>) and 0.65 (95% CI 0.58–0.72, *p* = 5.1 \* 10<sup>-5</sup>) for pCT and CBCT imaging, respectively.

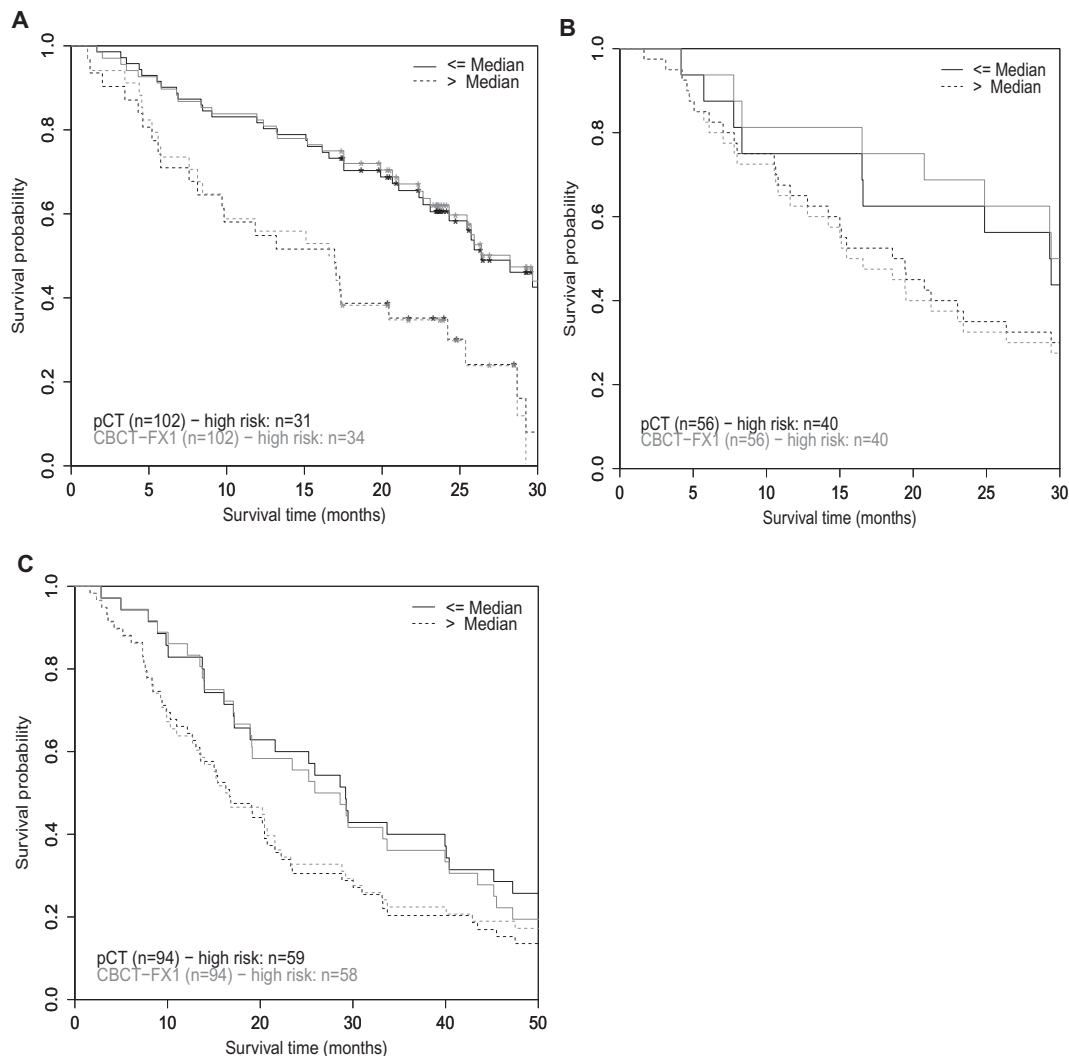


**Fig. 4.** Kaplan–Meier curves for pCT and CBCT. Kaplan–Meier curves are based on model predictions of the radiomic signature, split by a median prediction threshold derived by Aerts et al. [20]: (A) Dataset 1, (B) Dataset 2 and (C) Dataset 3.

## Discussion

A small proportion (13.3%) of radiomic features retrieved from planning CT are interchangeable with those retrieved from cone beam CT's. This group of features did include all features from the previously published prognostic radiomic signature [20]. Moreover, we tested its prognostic value in all three cohorts for pCT as well as CBCT. The similarity of linear predictors, after the two-step correction method, estimated by the Cox model of the radiomic signature shows that prognostic information can be obtained interchangeably from pCT or CBCT images. It has already been shown that image features derived from CBCT can potentially serve as an early biomarker for assessing response to treatment [27,28]. To the best of our knowledge, only one study investigated the potential of CBCT imaging in the field of radiomics [29]. However, these authors only performed test–retest analyses to assess the reproducibility of radiomic features obtained from CBCT imaging. The current study shows that a subset of radiomic features and the prognostic value of the radiomic signature are interchangeable between pCT and CBCT, showing the potential for using radiomics on CBCT imaging.

Kaplan–Meier curves of pCT and CBCT images are very similar for all datasets after correction, indicating that the same information can be derived from kV cone-beam CT images as from conventional spiral planning CT. Differences between the Kaplan–Meier curves between datasets could be explained by differences in cohorts, e.g. tumors were on average larger in dataset 2 and 3 (109.2 cm<sup>3</sup> and 71.1 cm<sup>3</sup> vs. 42.2 cm<sup>3</sup>) and also more stage III patients were included compared to dataset 1. More similar Kaplan–Meier curves are expected when cohorts are more comparable in both size and characteristics. For dataset 2, the non-significant split of the Kaplan–Meier curves could potentially be explained by the low number of patients (16 out of 56) in the high prognostic group.

In this study, overall survival was analyzed as outcome. Although this outcome is highly relevant for patients, its association with imaging features is expected to be less strong than local tumor control or disease progression. Using this outcome, the prognostic performance of pCT as well as CBCT might increase.

There are several challenges in using CBCT imaging for radiomics. Extracted textural features typically depend on reconstruction and scanning parameters [29–32]. Therefore, to be consistent throughout this study, only CBCT images with a 3 mm slice thickness were included in dataset 1, which is identical to the slice thickness in the pCT images. Nonetheless, the CBCTs of dataset 2 and 3 all had a slice thickness of 1 mm, which could partly explain the differences in linear regression parameters and model validation results between datasets. After resampling all slice thicknesses into an equal size of 3 mm, energy features of CBCT images of dataset 2 and 3 decreased by a factor 3, as expected since energy is directly related to the number of voxels. The resampling resulted in more similar results between datasets in terms of linear regression parameters. However, the influence of slice thickness on the radiomic feature values needs further investigation [33]. Furthermore, other unknown factors might influence the interchangeability between pCT and CBCT radiomics or the consistency of radiomics' performance on CT images. Potentially, a radiomics approved reconstruction or corrections afterward as performed in this study, could in general improve the consistency and utility of radiomics in medical imaging.

Besides this, the detector size of the cone-beam CT has a limited field of view (FOV) that may not be large enough for extensive tumors and off-axis patient positions. Moreover, for calculating filtered radiomic features, a certain margin is necessary to avoid padding with artificial values. These issues could potentially be solved

by stitching together two acquisitions, or extracting radiomic features using the image slice with the largest tumor cross section, which should still be investigated for CBCT imaging [10,34].

Other challenges with CBCT images for radiomics include their increased noise and sensitivity to (strike) artifacts compared to conventional CT images. Due to the prolonged scan time of approximately one minute, CBCT images are more susceptible for motion artifacts. Respiratory correlated CT imaging minimizes the breathing artifacts, which is not the case for respiration-averaged CBCT images. Four-dimensional (4D) CBCT imaging might overcome this problem, however possible decreased image quality and increased noise compared to 3D CBCT imaging [35] may be observed and 4D CBCT images are typically not acquired in routine clinical practice. More research is needed to investigate the influence of artifacts in CBCT radiomics.

This study shows that after applying correction, comparable prognostic information can be derived from CBCT images as from CT images for NSCLC patients. Apparently, the radiomic signature is a subset of features that is able to derive the important prognostic information which is not affected by differences in image acquisition and reconstruction between CT and CBCT. When performing radiomics, one should perform extensive test–retest and stability analyses to select most reliable imaging features, which is especially important when using lower quality images like cone-beam CT. In the future, new models can be developed based on CBCT extracted radiomic features in combination with other (clinical) parameters that potentially have improved prognostic performance. Developing new models was outside the scope of the current study.

Since multiple scans are routinely made in clinical practice, CBCT imaging could potentially be used in a longitudinal fashion to develop so-called “delta radiomics”. Tumor changes occurring over the course of treatment, e.g. cell death, accelerated proliferation and reoxygenation, could then be monitored using radiomics metrics. Since this study only shows the interchangeability with planning CT radiomics, further research is needed to explore the performance of delta radiomic features extracted from kV cone-beam CT images for the (improved) prediction of survival and/or to quantify accelerated proliferation as a predictor for local progression.

## Conclusion

This study shows that a selection of radiomic features are interchangeable when extracted from either planning CT or cone-beam CT images. The performance of the previously developed CT-based radiomic signature on CBCT images shows that prognostic information on overall survival can be derived from CBCT images of non-small cell lung cancer patients acquired prior to the first fraction of treatment, providing a two-step correction procedure was performed. These results show great potential for the use of radiomics on CBCT images. CBCT radiomics can now be further evaluated for its potential to monitor tumor changes over the course of treatment (the so-called “delta radiomics” approach).

## Conflict of interest statement

Ralph T.H. Leijenaar is a salaried employee of ptTheragnostic B. V., which develops products for patient stratification for personalized radiotherapy.

## Acknowledgements

This work was supported by the ERC advanced grant (ERC-ADG-2015, n° 694812 – Hypoximmuno) and the QuIC-ConCePT project,

which is partly funded by EFPI A companies and the Innovative Medicine Initiative Joint Undertaking (IMI JU) under Grant Agreement No. 115151. This research is also supported by the Dutch Technology Foundation STW (grant n° 10696 DuCAT & n° P14-19 Radiomics STRaTegy), which is the applied science division of NWO, and the Technology Programme of the Ministry of Economic Affairs. Authors also acknowledge financial support from the EU 7th framework program (ARTFORCE – n° 257144, REQUITE – n° 601826), SME Phase 2 (EU proposal 673780 – RAIL), the European Program H2020-2015-17 (BD2Decide – PHC30-689715 and ImmunoSABR – n° 733008), Interreg V-A Euregio Meuse-Rhine (“Eura-diagnostics”), Kankeronderzoekfonds Limburg from the Health Foundation Limburg, Alpe d’HuZes-KWF (DESIGN), EUROSTARS (DART) and the Dutch Cancer Society. Authors thank the contribution of Anisha Gogineni for editing.

## Appendix A. Supplementary data

Supplementary data associated with this article can be found, in the online version, at <http://dx.doi.org/10.1016/j.radonc.2017.04.016>.

## References

- [1] Torre LA, Bray F, Siegel RL, Ferlay J, Lortet-Tieulent J, Jemal A. Global cancer statistics, 2012. *CA Cancer J Clin* 2015;65:87–108.
- [2] Ferlay J, Soerjomataram I, Dikshit R, et al. Cancer incidence and mortality worldwide: sources, methods and major patterns in GLOBOCAN 2012. *Int J Cancer* 2015;136:E359–86.
- [3] Lambin P, van Stiphout RG, Starmans MH, et al. Predicting outcomes in radiation oncology—multifactorial decision support systems. *Nat Rev Clin Oncol* 2013;10:27–40.
- [4] Lambin P, Roelofs E, Reymen B, et al. Rapid Learning health care in oncology’ – an approach towards decision support systems enabling customised radiotherapy. *Radiother Oncol* 2013;109:159–64.
- [5] Lambin P, Zindler J, Vanneste BG, et al. Decision support systems for personalized and participative radiation oncology. *Adv Drug Deliv Rev* 2016.
- [6] Oberije C, De Ruyscher D, Houben R, et al. A validated prediction model for overall survival from stage III non-small cell lung cancer: toward survival prediction for individual patients. *Int J Radiat Oncol Biol Phys* 2015;92:935–44.
- [7] Oberije C, Nalbantov G, Dekker A, et al. A prospective study comparing the predictions of doctors versus models for treatment outcome of lung cancer patients: a step toward individualized care and shared decision making. *Radiother Oncol* 2014;112:37–43.
- [8] Carvalho S, Leijenaar RT, Velazquez ER, et al. Prognostic value of metabolic metrics extracted from baseline positron emission tomography images in non-small cell lung cancer. *Acta Oncol* 2013;52:1398–404.
- [9] Fried DV, Tucker SL, Zhou S, et al. Prognostic value and reproducibility of pretreatment CT texture features in stage III non-small cell lung cancer. *Int J Radiat Oncol Biol Phys* 2014;90:834–42.
- [10] Ganeshan B, Panayiotou E, Burnand K, Dizdarevic S, Miles K. Tumor heterogeneity in non-small cell lung carcinoma assessed by CT texture analysis: a potential marker of survival. *Eur Radiol* 2012;22:796–802.
- [11] Coroller TP, Grossmann P, Hou Y, et al. CT-based radiomic signature predicts distant metastasis in lung adenocarcinoma. *Radiother Oncol* 2015;114:345–50.
- [12] Lambin P, Rijs-Velazquez E, Leijenaar R, et al. Radiomics: extracting more information from medical images using advanced feature analysis. *Eur J Cancer* 2012;48:441–6.
- [13] Kumar V, Gu Y, Basu S, et al. Radiomics: the process and the challenges. *Magn Reson Imaging* 2012;30:1234–48.
- [14] Gillies RJ, Kinahan PE, Hricak H. Radiomics: images are more than pictures, they are data. *Radiology* 2016;278:563–77.
- [15] Aerts HJ, Grossmann P, Tan Y, et al. Defining a radiomic response phenotype: a pilot study using targeted therapy in NSCLC. *Sci Rep* 2016;6:33860.
- [16] Cunliffe A, Armato 3rd SG, Castillo R, Pham N, Guerrero T, Al-Hallaq HA. Lung texture in serial thoracic computed tomography scans: correlation of radiomics-based features with radiation therapy dose and radiation pneumonitis development. *Int J Radiat Oncol Biol Phys* 2015;91:1048–56.
- [17] Antunes J, Viswanath S, Rusu M, et al. Radiomics analysis on FLT-PET/MRI for characterization of early treatment response in renal cell carcinoma: a proof-of-concept study. *Transl Oncol* 2016;9:155–62.
- [18] Jaffray DA, Siewerdsen JH, Wong JW, Martinez AA. Flat-panel cone-beam CT for image-guided radiation therapy. *Int J Radiation Oncology Biol Psychol* 2002;53:1337–49.
- [19] Brink C, Bernchou U, Bertelsen A, Hansen O, Schytte T, Bentzen SM. Locoregional control of non-small cell lung cancer in relation to automated early assessment of tumor regression on cone beam computed tomography. *Int J Radiat Oncol Biol Phys* 2014;89:916–23.
- [20] Aerts HJ, Velazquez ER, Leijenaar RT, et al. Decoding tumour phenotype by noninvasive imaging using a quantitative radiomics approach. *Nat Commun* 2014;5:4006.
- [21] Leijenaar RT, Carvalho S, Hoebbers FJ, et al. External validation of a prognostic CT-based radiomic signature in oropharyngeal squamous cell carcinoma. *Acta Oncol* 2015;54:1423–9.
- [22] van Timmeren JE, Leijenaar RTH, van Elmpt W, et al. Data from: Survival prediction of non-small cell lung cancer patients using radiomics analyses of cone-beam CT images; 2017. <http://dx.doi.org/10.17195/candat.2017.02.1>.
- [23] Moteabbed M, Sharp GC, Wang Y, Trofimov A, Efsthathiou JA, Lu H-M. Validation of a deformable image registration technique for cone beam CT-based dose verification. *Med Phys* 2015;42:196–205.
- [24] Veiga C, McClelland J, Moinuddin S, et al. Toward adaptive radiotherapy for head and neck patients: Feasibility study on using CT-to-CBCT deformable registration for “dose of the day” calculations. *Med Phys* 2014;41:031703.
- [25] Cardiac CT. Imaging diagnosis of cardiovascular disease. Berlin Heidelberg, New York, NY: Springer; 2016.
- [26] Royston P, Altman DG. External validation of a Cox prognostic model, principles and methods. *BMC Med Res Methodol* 2013;13.
- [27] Bertelsen A, Schytte T, Bentzen SM, Hansen O, Nielsen M, Brink C. Radiation dose response of normal lung assessed by Cone Beam CT – a potential tool for biologically adaptive radiation therapy. *Radiother Oncol* 2011;100:351–5.
- [28] Bernchou U, Hansen O, Schytte T, et al. Prediction of lung density changes after radiotherapy by cone beam computed tomography response markers and pre-treatment factors for non-small cell lung cancer patients. *Radiother Oncol* 2015;117:17–22.
- [29] Fave X, Mackin D, Yang J, et al. Can radiomics features be reproducibly measured from CBCT images for patients with non-small cell lung cancer? *Med Phys* 2015;42:6784.
- [30] Mackin D, Fave X, Zhang L, et al. Measuring computed tomography scanner variability of radiomics features. *Invest Radiol* 2015;50:757–65.
- [31] Balagurunathan Y, Gu Y, Wang H, et al. Reproducibility and prognosis of quantitative features extracted from CT images. *Transl Oncol* 2014;7:72–87.
- [32] Balagurunathan Y, Kumar V, Gu Y, et al. Test–retest reproducibility analysis of lung CT image features. *J Digit Imaging* 2014;27:805–23.
- [33] Zhao B, Tan Y, Tsai WY, et al. Reproducibility of radiomics for deciphering tumor phenotype with imaging. *Sci Rep* 2016;6:23428.
- [34] Ganeshan B, Goh V, Mandeville HC, Ng QS, Hoskin PJ, Miles KA. Non-small cell lung cancer: histopathologic correlates for texture parameters at CT. *Radiology* 2013;266:326–36.
- [35] Lee S, Yan G, Lu B, Kahler D, Li JG, Sanjiv SS. Impact of scanning parameters and breathing patterns on image quality and accuracy of tumor motion reconstruction in 4D CBCT: a phantom study. *J Appl Clin Med Phys*. 2015;16.